Simulation Study of Trapped Electron Effects on Positron Acceleration by a Shock Wave in an Electron-Ion-Positron Plasma

Mieko Toida

National Institute for Fusion Science, Toki 509-5292, Japan

Positron acceleration by a shock wave in an electro-ion-positron plasma is studied with a two-dimensional, relativistic, electromagnetic particle simulation, with special attention to effects of electrons trapped in the shock wave. It is demonstrated that ultrarelativistic positron acceleration can occur even when the fluctuations along the shock front, which we call 2D fluctuations, excited by the trapped electrons grow to large amplitudes. Further, by comparing the results of the simulation and the calculation of test positrons not influenced by the 2D fluctuations, we show that the positrons influenced by the 2D fluctuations are accelerated to higher energies than the positrons not influenced by them. In addition to the parallel electric field formed in the shock transition region, the perpendicular electric field in the shock wave greatly contributes to the ultrarelativistic positron acceleration under the influence of the 2D fluctuations. Effects of the accelerated positrons on the 2D fluctuations are also discussed.

1. Introduction

Formation of a collisionless shock wave and associated particle acceleration are complex phenomena involving nonlinear interaction between large-amplitude waves and particles.[1,2] Therefore, relativistic electromagnetic particle simulations that solve evolution of electromagnetic fields and relativistic particle motions in a self-consistent manner give us important information on the particle acceleration by a collisionless shock wave. In fact, the particle simulations have revealed various acceleration mechanisms depending on particle species, propagation condition of the shock wave, and the strength of the external magnetic field (Ref. 3 and references therein).

For example, a magnetosonic shock wave propagating obliquely to the external magnetic field can trap some electrons and can rapidly accelerate them by the strong electric fields formed near the shock front.[4] The energies of the accelerated electrons can be ultrarelativistic when the external magnetic field is strong such that $|\Omega_e|/\omega_{pe} > 1$, where Ω_e and ω_{pe} are the electron cyclotron and plasma frequencies, respectively, and the propagation speed of the

shock wave $v_{\rm sh}$ is close to $c\cos\theta$, where c is the speed of light and θ is the propagation angle of the shock wave.[5] The magnetosonic shock wave with $v_{\rm sh} \simeq c\cos\theta$ in the strong external magnetic field can also accelerate positrons to ultrarelativistic energies when the plasma consists of ions, electrons, and positrons and the positron density is low.[6,7] In the ultrarelativistic positron acceleration, the electric field parallel to the magnetic field formed in the shock transision region plays an essential role. This result may be applicable to positron acceleration around pulsars because positrons are suspected to exist around the pulsars with the strong magnetic fields,[8,9] and the pulsars have been discussed as one of the sources of cosmic-ray positrons (for example, Refs. 10, 11 and references therein).

Particles accelerated by the shock wave can cause various instabilities. The instabilities can affect electromagnetic fields and particle motions in the shock wave. This nonlinear evolution of the instabilities is also an important issue that should be solved by the particle simulations. Especially, we note effects of the electrons trapped in the oblique shock wave with $v_{\rm sh} \simeq c\cos\theta$ because such electrons cannot readily escape from the shock wave and the number of the trapped electrons increases with time.[12] In fact, the two-dimensional (2D) particle simulations have shown that the electromagnetic fluctuations with finite wavenumbers along the shock front, which we call 2D fluctuations, grow to large amplitudes as a result of the nonlinear development of the oblique-whistler wave instabilities driven by the trapped electrons.[13,14] The 2D fluctuations can significantly influence the electron acceleration.

As described above, the electron trapping and the ultrarelativistic positron acceleration can occur simultaneously in the shock wave with $v_{\rm sh} \simeq c\cos\theta$ in the electron-ion-positron plasma. Therefore, we can expect that the trapped electrons would influence positron motions in the shock wave. However, this has not been studied because the simulations of the ultrarelativistic positron acceleration[6,7,15,16] were performed with the one-dimensional simulations in which the 2D fluctuations excited by the trapped electrons are not included. By using the two-dimensional simulations in which the 2D fluctuations excited by the trapped electrons are included, we should investigate whether the ultrarelativistic positron acceleration can occur or not even in the situation where the instabilities driven by the trapped electrons are strongly involved. Further, if it occurs, we should clarify how the trapped electrons influence the positron energy and the positron acceleration mechanism.

In this paper, we study effects of the trapped electrons on the positron acceleration in the shock wave by using the 2D particle simulations. It is demonstrated that positrons can be accelerated to ultrarelativistic energies even when the 2D fluctuations excited by the trapped electrons grow to large amplitudes. Further, it is found that the positrons influenced by the

2D fluctuations can be accelerated to higher energies than the positrons not influenced by the 2D fluctuations. As for the acceleration mechanism, it is shown that in addition to the electric field parallel to the magnetic field $E_\parallel$ in the shock transition region, the perpendicular electric field $E_\perp$ in the shock wave greatly contributes to the positron acceleration when the amplitudes of the 2D fluctuations are large.

In Sec. II, we describe the simulation model and parameters. In order to analyze the positron motions under the influence of the 2D fluctuations in detail, we follow the orbits of many positrons in the 2D simulation. We call these positrons 2Ds positrons. We also calculate the orbits of the same number of the test positrons in the electromagnetic fields averaged along the shock front. That is, the test positrons, which we call 1Dt positrons, are not influenced by the 2D fluctuations excited by the trapped electrons.

In Sec. III, we present the simulation results. It is demonstrated that the 2Ds positrons are accelerated to ultrarelativistic energies even under the influence of the large-amplitude 2D fluctuations. Further, by comparing the 2Ds positrons and the 1Dt positrons, we elucidate effects of the 2D fluctuations on the accelerated positron energy and distribution. We also discuss the difference between the acceleration mechanisms of the 1Dt positrons and the 2Ds positrons. It is shown that the 2Ds positrons that are accelerated to higher energies tend to obtain energies from $E_\perp$ more than from $E_\parallel$. At the end of Sec. III, we discuss effects of the accelerated positrons on 2D fluctuations. Section IV gives a summary of our work.

2. Simulation Model and Parameters

We study positron acceleration by an oblique shock wave in an electron-ion-positron plasma by using a 2D (two spatial coordinates and three velocity components), relativistic, electromagnetic particle code which self-consistently calculates full dynamics of electrons, ions, and positrons and evolution of electromagnetic fields. We pay attention to effects of electrons trapped in the main pulse of the shock wave. Here, the main pulse designates the first leading pulse in a shock wave because the shock wave approximates the train of solitons with decreasing amplitudes when the dissipation is small.[1,2] The stable electron trapping was observed in the 1D simulations of such a shock wave with $v_{\rm sh} \simeq c\cos\theta$ in the strong magnetic field $\Omega_{\rm e}/\omega_{\rm pe} > 1$.[12] Also, the strong positron acceleration by such a shock wave in an electron-ion-positron plasma was observed in the 1D simulations when the positron density is rather low $n_p/n_e \leq 0.1$.[7] Therefore, we choose the parameters of the 2D simulation close to the parameters of the 1D simulations in order to investigate effects of the trapped electrons on the positron acceleration.

We simulate an oblique shock wave propagating in the x direction in an external magnetic field in the (x, z) plane, $\boldsymbol{B}_0 = B_0(\cos\theta, 0, \sin\theta)$ with $\theta = 54°$. We set the simulation plane as (x, y) because 2D fluctuations along the shock front grow to large amplitudes in the (x, y) plane, as a result of nonlinear development of oblique whistler-wave instabilities driven by trapped electrons.[14] As shown in Ref. 14, when the external magnetic field $\boldsymbol{B}_0$ is in the (x, y) plane, 2D fluctuations do not grow to large amplitudes because the nonlinear evolution of the instabilities is suppressed. We therefore make $\boldsymbol{B}_0$ in the (x, z) plane.

The simulation system size is $L_x \times L_y = 16384\Delta_g \times 512\Delta_g$, where Δ_g is the grid spacing. The total number of electrons is $N \simeq 1.1 \times 10^9$. The system is periodic in the y direction. As for the x direction, the particles are confined in the region $200\Delta_g < x < L_x - 200\Delta_g$, being reflected at these boundaries.[17] The ion-to-electron mass ratio is $m_i/m_e = 400$. In the upstream region, the electron and positron thermal velocities are $v_{Te} = v_{Tp} = 0.5(\omega_{pe}\Delta_g)$, and the ion thermal velocity $v_{Ti} = 0.025(\omega_{pe}\Delta_g)$. The light speed is $c/(\omega_{pe}\Delta_g) = 4$. In order to simulate a shock wave in the strong magetic field, we set the ratio of Ω_e to ω_{pe} in the upstream region as $|\Omega_e|/\omega_{pe} = 5.0$. The Alfvén speed is $v_A/(\omega_{pe}\Delta_g) = 1.0$. The propagation speed of the shock wave is $v_{sh} = 0.95c\cos\theta$ and the Alfvén Mach number is $M_A = 2.3$. The results for the shock waves with $v_{sh} = 0.90c\cos\theta$ and $1.05c\cos\theta$ are presented in Appendix. The method of excitation of the shock wave is described in Ref. 13.

We assume that the positron-to-electron mass density ratio is $n_p m_p/(n_e m_e) = 0.02$. To have good statistics for positrons with the small density, we use the fine particle method as in Ref. 16. Keeping the relation $m_p/q_p = m_e/e$, where q_p is the positron charge, and $n_p m_p/(n_e m_e) = 0.02$, we set the positron mass to be small, $m_p = m_e/10$, and increase the number of positrons by 10 times. The positron plasma frequency and the positron cyclotron frequency are unchanged by this.

In order to elucidate the effects of 2D fluctuations on positron motions, we compute the orbits of test positrons that are in the electromagnetic fields averaged along the y direction. We integrate the relativistic equation of motion for the test positrons,

$$\frac{d\boldsymbol{P}}{dt} = e\bar{\boldsymbol{E}}(x,t) + \frac{e}{c}\boldsymbol{v} \times \bar{\boldsymbol{B}}(x,t). \tag{1}$$

Here, $\bar{\boldsymbol{E}}$ and $\bar{\boldsymbol{B}}$ are the 1D electromagnetic fields defined as

$$\bar{\boldsymbol{E}} = \frac{1}{L_y}\int_0^{L_y} dy\boldsymbol{E}(x,y,t), \quad \bar{\boldsymbol{B}} = \frac{1}{L_y}\int_0^{L_y} dy\boldsymbol{B}(x,y,t), \tag{2}$$

where $\boldsymbol{E}(x, y, t)$ and $\boldsymbol{B}(x, y, t)$ are obtained by the 2D electromagnetic particle simulation. We write the test positrons as 1Dt positrons. The 1Dt positrons are not under the influence

of the 2D fluctuations excited by the trapped electrons. The number of the 1Dt positrons is 4.2×10^6. We also follow the same number of positrons in the 2D simulation, which we call 2Ds positrons. The 1Dt positrons and the 2Ds positrons have the same initial positions and velocities. Comparison between the two groups of positrons will show influences of 2D fluctuations on positron motions in an oblique shock wave.

3. Simulation Results

3.1 Positron distributions

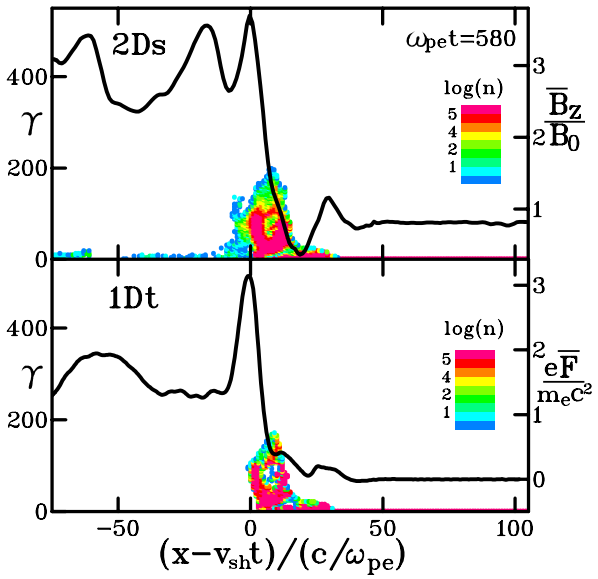

Fig. 1. Phase spaces (x, γ) of the 2Ds positrons and the 1Dt positrons and the x profile of the y-averaged magnetic field $\bar{B}_z$ and the parallel pseudo-potential $\bar{F}$ given by eq. (3) at $\omega_{pe}t = 580$. (Color online)

We first show that the 2Ds positrons can be strongly accelerated by a shock wave even under the influence of the 2D fluctuations and the energies of the accelerated 2Ds positrons are higher than those of the accelerated 1Dt positrons.

Figures 1 and 2 show the phase spaces (x, γ), where γ is the Lorentz factor, of 2Ds positrons and 1Dt positrons at $\omega_{pe}t = 580$ and 2980, respectively. The color indicates the number density in the (x, γ) plane, which is averaged over the y direction. The x position of the shock front is $x - v_{sh}t = 0$. The solid line in the upper panel shows the x profile of the y-averaged magnetic field $\bar{B}_z$. The solid line in the lower parallel shows $\bar{F}$ defined as

$$\bar{F} = -\int \frac{\bar{\boldsymbol{E}} \cdot \bar{\boldsymbol{B}}}{\bar{B}} d\bar{s} = -\int \left(\frac{\bar{E}_{\parallel} \bar{B}}{B_{x0}} \right) dx, \tag{3}$$

where $\bar{s}$ is the length along the 1D magnetic field $\bar{\boldsymbol{B}}$ and $d\bar{s} = dx\bar{B}/B_{x0}$. We call $\bar{F}$ the

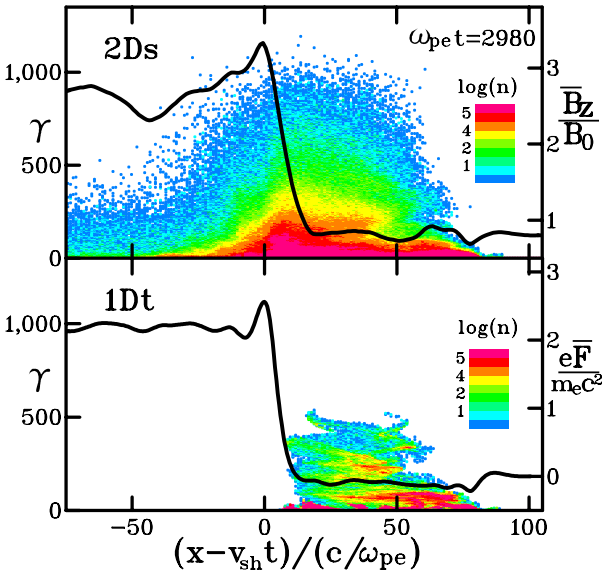

Fig. 2. Phase spaces (x, γ) of the 2Ds positrons and the 1Dt positrons and the x profile of the magnetic field $\bar{B}_z$ and the parallel pseudo-potential $\bar{F}$ at $\omega_{pe}t = 2980$. (Color online)

parallel pseudo-potential for the 1D electromagnetic fields. When the external magnetic field is strong, the strong $E_\parallel$ can be formed in the shock transition region[18,19] and the maximum value of $\bar{F}$ becomes greater than $m_e c^2$. The strong $E_\parallel$ plays an essential role in the positron acceleration,[6,7] which we will show in more detail below.

Figures 1 and 2 show that both the 2Ds positrons and the 1Dt positrons are accelerated to ultrarelativistic energies such as $\gamma > 100$. This indicates that the ultrarelativistic positron acceleration by the shock wave can occur even under the influence of the 2D fluctuations excited by the trapped electrons. Further, we see the difference between the distributions of the two groups of positrons. At $\omega_{pe}t = 580$ (see Fig. 1), almost all the energetic 1Dt positrons, which are accelerated near the shock front, are in the region $x > v_{sh}t$ and few energetic 1Dt positrons are in the region $x < v_{sh}t$. On the other hand, some energetic 2Ds positrons exist in the region $x < v_{sh}t$, in addition to many energetic 2Ds positrons in the region $x > v_{sh}t$. The difference between the distributions of the 2Ds positrons and the 1Dt positrons is much greater at $\omega_{pe}t = 2980$ (Fig. 2) than at $\omega_{pe}t = 580$. We see no energetic 1Dt positrons in the region $x < v_{sh}t$. The number of the energetic 1Dt positrons in the region $x > v_{sh}$ is larger at $\omega_{pe}t = 2980$ than at $\omega_{pe}t = 580$. This indicates that almost all the 1Dt positrons that encountered the shock wave are accelerated near the shock front and are then reflected to the upstream region $x > v_{sh}t$. On the other hand, the accelerated 2Ds positrons are distributed over a wide region from the upstream to the downstream of the shock wave. Further, the

values of γ of the 2Ds positions are higher than those of the 1Dt positrons. The maximum γ of the 2Ds positrons is $\gamma_{\rm M} \sim 1000$, whereas that of the 1Dt positrons is $\gamma_{\rm M} \sim 500$.

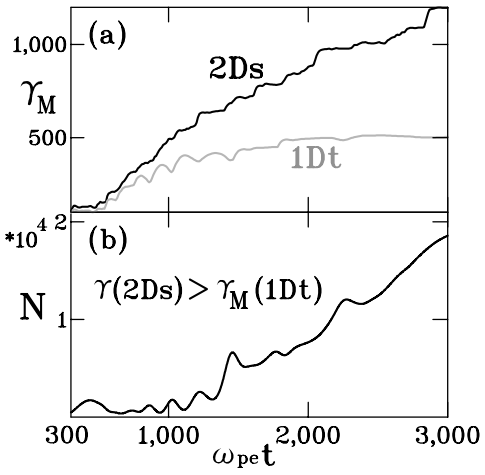

Fig. 3. Time variations of the maximum γ values of the 2Ds positrons and the 1Dt positrons (a) and time variation of the number of the 2Ds positions accelerated to higher energies than the 1Dt positrons (b).

The upper panel in Fig. 3 presents the time variations of the maximum γ of the 2Ds positrons (black line) and that of the 1Dt positrons (gray line). The difference between the $\gamma_{\rm M}$ values of the 2Ds positrons and the 1Dt positrons is small in the early stage, $\omega_{\rm pe}t < 1000$. However, after $\omega_{\rm pe}t \simeq 1000$, the difference increases with time. The lower panel in Fig. 3 shows the time variation of the number of the 2Ds positrons having γ greater than $\gamma_{\rm M}$ of the 1Dt positrons, that is, the number of the 2Ds positrons accelerated to higher energies than the 1Dt positrons. This number also increases with time after $\omega_{\rm pe}t \simeq 1000$. Thus, we see that after $\omega_{\rm pe}t \simeq 1000$, the acceleration of the 2Ds positrons is considerably enhanced compared to the acceleration of the 1Dt positrons.

3.2 2D fluctuation amplitude

The difference between the 2Ds positrons and the 1Dt positrons are caused by the 2D fluctuations excited by the trapped electrons. In order to confirm this, we plot, with the black line in Fig. 4(a), the time variation of the 2D fluctuation amplitude averaged over the shock

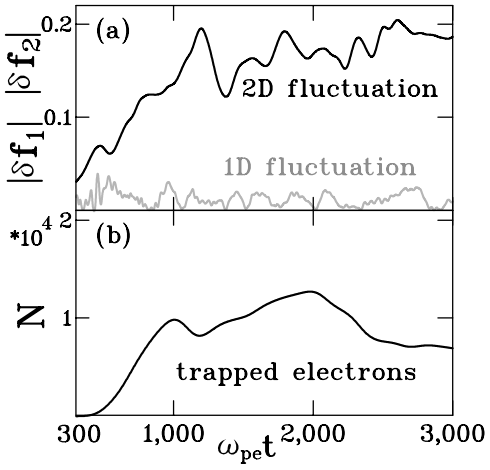

Fig. 4. (a) Time variations of the 2D fluctuation amplitude (black line) and the 1D fluctuation amplitude (gray line). The values of $|\delta f_1|$ and $|\delta f_2|$ are normalized by B_0. (b) Time variation of the number of trapped electrons.

transision region, $|\delta f_2|$, which is defined by

$$|\delta f_2| = \frac{1}{L_y d_x} \int_0^{L_y} dy \int_{x_m}^{x_m+d} dx(|\delta \boldsymbol{E}_2(x,y,t)| + |\delta \boldsymbol{B}_2(x,y,t)|). \tag{4}$$

Here, x_m is the x position at which $\bar{B}_z$ becomes maximum, $x_m \simeq v_{\rm sh}t$, and d is the width of the shock transition region, and $\delta \boldsymbol{E}_2$ and $\delta \boldsymbol{B}_2$ are 2D fluctuations,

$$\delta \boldsymbol{E}_2(x,y,t) = \boldsymbol{E}(x,y,t) - \bar{\boldsymbol{E}}(x,t), \quad \delta \boldsymbol{B}_2(x,y,t) = \boldsymbol{B}(x,y,t) - \bar{\boldsymbol{B}}(x,t). \tag{5}$$

The gray line in Fig. 4 (a) shows the 1D fluctuation amplitude at $x = x_m$, which is defined by

$$|\delta f_1| = \left| \bar{\boldsymbol{B}}(x_m,t) - \frac{1}{T}\int_{t_1}^{t_2} dt \bar{\boldsymbol{B}}(x_m,t) \right| + \left| \bar{\boldsymbol{E}}(x_m,t) - \frac{1}{T}\int_{t_1}^{t_2} dt \bar{\boldsymbol{E}}(x_m,t) \right|, \tag{6}$$

where $\omega_{\rm pe}t_1 = 300$, $\omega_{\rm pe}t_2 = 3000$, and $T = t_2 - t_1$. The 1D fluctuation amplitude is due to the nonstationarity of the shock wave. Figure 4 (a) clearly shows that the 2D fluctuation amplitude $|\delta f_2|$ is much greater than that of the 1D fluctuation amplitude $|\delta f_1|$. Comparing Fig. 3 and Fig. 4(a), we confirm that the difference between the two groups of positrons increases when $|\delta f_2|$ is large.

As discussed in Ref. 14, the 2D fluctuations are caused by the electrons trapped in the main pulse of the shock wave. (The electron phase space plot will be shown below.) Figure 4 (b) shows the time variation of the number of trapped electrons. The value of $N(t)$ indicates the number of electrons that are being trapped in the main pulse at the time t, and the electrons that have been detrapped from the main pulse by the time t are not included in this number. Comparing Figs. 4 (a) and (b), we see that when the number of the trapped electrons is large,

the 2D fluctuation amplitude $|\delta f_2|$ is large on average. However, looking at the variations after $\omega_{\rm pe}t \simeq 2000$ in detail, although the number of trapped electrons gradually decreases due to the electron detrapping from the main pulse, $|\delta f_2|$ remains large. This may be effects of the accelerated positrons. At the end of this section, we discuss effects of the accelerated positrons on the 2D fluctuations.

3.3 Positron orbits

In this subsection, we show typical orbits of accelerated positrons and consider effects of the 2D fluctuations on the positron acceleration mechanisms.

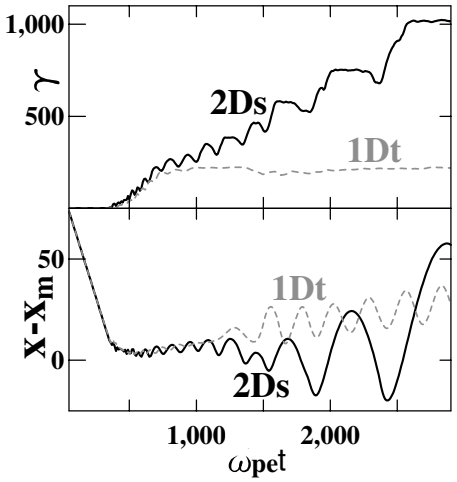

Fig. 5. Comparison between the 2Ds positron (black line) and the 1Dt positron (gray dashed line) that have the same initial position and velocity. Time variations of γ and $x - x_m$ of the two positrons are plotted, where x_m is the shock wave position. The values of $x - x_m$ are normalized by $c/\omega_{\rm pe}$.

The black solid lines in Fig. 5 show the time variations of γ and the position $x - x_m$ of the 2Ds positron accelerated to $\gamma > 1000$. Here, the value of $x - x_m$ is normalized by $c/\omega_{\rm pe}$. The gray dashed lines in Fig. 5 show the values of the 1Dt positron that has the same initial position and velocity as the 2Ds positron shown by the black solid line. At $\omega_{\rm pe}t \simeq 300$, both the 2Ds positron and the 1Dt positron encounter the shock wave and the values of γ begin to increase. The acceleration of the 1Dt positron ends at $\omega_{\rm pe}t \simeq 750$, and the 1Dt positron has then never entered the region behind the shock front $x < x_m$. On the other hand, the 2Ds

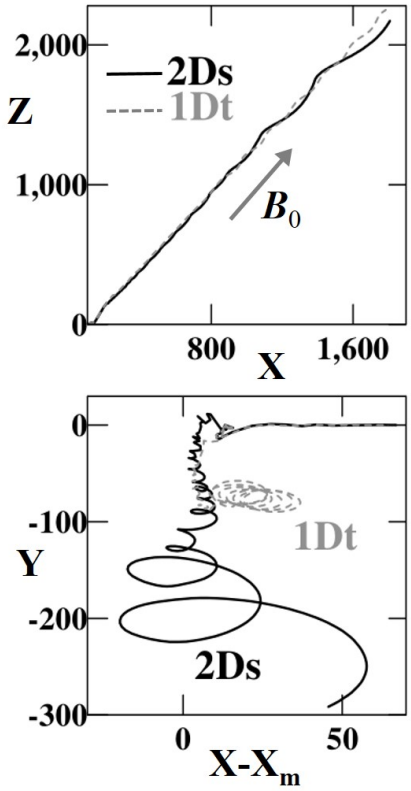

Fig. 6. The 2Ds positron orbit (black line) and the 1Dt positron orbit (gray dashed line) in the (x, z) and $(x - x_{\rm m}, y)$ planes. The values of x, y, and z are normalized by $c/\omega_{\rm pe}$

positron enters and exits the region $x < x_m$ several times after $\omega_{\rm pe}t \simeq 1000$. In association with this motion, the value of γ of the 2Ds positron rises stepwise.

Figure 6 displays the orbits of the two positrons in the (x, y) plane and (x, z) plane for the period from $\omega_{\rm pe}t = 0$ to 3000, where the values of x, y, and z are normalized by $c/\omega_{\rm pe}$. The upper panel of Fig. 6 shows that the accelerated positrons move nearly parallel to the external magnetic field $\boldsymbol{B}_0$ with the speed $v_{\parallel} \simeq c$ and $v_x \simeq c\cos\theta$. Because the shock speed $v_{\rm sh}$ is close to $c\cos\theta$, both the 1Dt positron and the 2Ds positron stay near the shock front for a long period of time. However, the two positrons have different gyroradii after having encountered the shock wave. The lower panel of Fig. 6 shows that the 1Dt positron has the smaller gyroradius and stays slightly ahead of the shock front. On the other hand, the 2Ds positron has the larger gyroradius, and it enters and exits the region $x < x_m$ several times. In association with this gyromotion, the 2Ds positron is accelerated by the mechanism reported in Ref. 20 for accelerating energetic ions. That is, the 2Ds positron gains the energy from the transverse electric field E_y when it is in the region $x < x_m$ because the E_y is parallel to the gyromotion of the 2Ds positron. (In the laboratory frame, the profile of $\bar{E}_y$ is similar to that of $\bar{B}_z$, and $\bar{E}_y$ is positive in the shock wave and almost zero in the upstream region.[21–25]) This

process repeats three times after $\omega_{pe}t \simeq 1500$ as shown in the upper panel in Fig. 5.

As we will show below, the dominant mode of the 2D fluctuations has the wavelength along the y direction, $\lambda_y \simeq 10c/\omega_{pe}$. Because the gyroradius of the 2Ds positron after $\omega_{pe}t = 1500$ is greater than λ_y, we can expect that the later stage of the acceleration will not end if $v_{sh} \simeq c\cos\theta$ continues to be satisfied. As discussed in Ref. 14, the 2D fluctuations are due to quasi-perpendicular whistler waves excited by the trapped electrons, and the characteristic of the dominant mode can be roughly described by the linear theory for the quasi-perpendicular whistler waves. From this theory, we can obtain a relationship $\lambda_y/(c/\omega_{pe}) \propto |\Omega_e|/\omega_{pe}$ if the 2D fluctuation amplitude is assumed to be constant. This indicates that when $|\Omega_e|/\omega_{pe}$ is larger, λ_y might be greater than positron gyroradii. However, as Ω_e/ω_{pe} increases, $E_\parallel$ near the shock front becomes stronger.[18,19] Therefore, positrons can be firstly accelerated by the stronger $E_\parallel$ and can obtain higher energies. When such positrons are scattered by the 2D fluctuations, their gyroradii may be larger than λ_y. In the future, we will investigate the dependence of $|\Omega_e|/\omega_{pe}$ in detail.

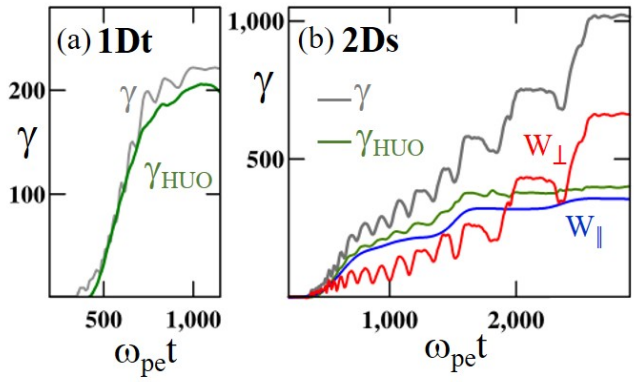

Fig. 7. (a) Comparison between the time variations of γ of the 1Dt positron and γ_{HU0} given by the theory (8) for the acceleration by a 1D stationary shock wave. (b) Time variations of γ of the 2Ds positron, γ_{HUO}, and works done by the parallel and perpendicular electric fields, $W_\parallel$ and $W_\perp$, for the 2Ds positron. The values of $W_\parallel$ and $W_\perp$ are normalized by $m_e c^2$. (Color online)

Figure 7 shows the comparison between the simulation result and the theory of ultrarelativistic positron acceleration by a one-dimensional shock wave presented in Ref. 7 where the positron acceleration mechanism was summarized as follows. Unlike the ion reflection by the shock wave,[26–28] positrons can be easily reflected by $E_\parallel$ in the shock transition region because the positron mass is small. When $v_{sh} \simeq c\cos\theta$, the reflected positrons with $v_\parallel \simeq c$ can stay near the shock front and can gain energies from $E_\parallel$ for a long period of time. As a

result, ultrarelativistic positrons can be produced. Under the assumption that the propagation speed of the shock wave is $v_{\rm sh} \simeq c\cos\theta$ and a positron moves nearly parallel to the external magnetic field with $v \simeq c$, the increase rate of the positron energy can be given by

$$\frac{d\gamma}{dt} = \Omega_{\rm p}\frac{c\cos\theta}{v_{\rm sh}}\frac{(\boldsymbol{E}\cdot\boldsymbol{B})}{(\boldsymbol{B}\cdot\boldsymbol{B}_0)}, \tag{7}$$

where $\Omega_{\rm p}$ is the positron cyclotron frequency. Figure 7 (a) displays the time variations of γ and $\gamma_{\rm HUO}$ of the 1Dt positron shown in Figs. 5 and 6 for the period from $\omega_{\rm pe}t = 300$ to 1200. (After $\omega_{\rm pe}t = 1200$, γ of the 1Dt positron does not change, as shown in Fig. 5.) Here, $\gamma_{\rm HUO}$ is defined as

$$\gamma_{\rm HUO} = \int \Omega_p\frac{c\cos\theta}{v_{\rm sh}}\frac{(\bar{\boldsymbol{E}}\cdot\bar{\boldsymbol{B}})}{(\bar{\boldsymbol{B}}\cdot\boldsymbol{B}_0)}dt, \tag{8}$$

where $\bar{\boldsymbol{E}}$ and $\bar{\boldsymbol{B}}$ are the 1D electromagnetic fields given by eq. (2) and the integration is carried out along the trajectory of the 1Dt positron. From fig. 7 (a), we confirm that the values of γ and $\gamma_{\rm HUO}$ are close for the 1Dt positron.

Figure 7 (b) shows the time variations of γ, $\gamma_{\rm HUO}$, $W_\parallel$, and $W_\perp$ for the 2Ds positron shown in Figs. 5 and 6. Here, in calculating $\gamma_{\rm HUO}$, the values of $\bar{\boldsymbol{E}}$ and $\bar{\boldsymbol{B}}$ at the x position of the 2Ds positron are used. $W_\parallel$ is the work done by the parallel electric field $E_\parallel$, and $W_\perp$ is the work done by the perpendicular electric field $E_\perp$, which is almost equal to E_y in the shock wave.[21–25] That is, $W_\parallel$ and $W_\perp$ are defined as

$$W_\parallel = \frac{e}{m_e c^2}\int \boldsymbol{E}_\parallel\cdot\boldsymbol{v}dt, \quad W_\perp = \frac{e}{m_e c^2}\int \boldsymbol{E}_\perp\cdot\boldsymbol{v}dt, \tag{9}$$

where $\boldsymbol{v}$ is the positron velocity. The values of $W_\parallel$ and $W_\perp$ in Fig. 7 (b) are normalized to $m_e c^2$. In the early stage such that $\omega_{\rm pe}t < 1000$, the values of γ, $\gamma_{\rm HUO}$, and $W_\parallel$ are close and they are much greater than $W_\perp$. However, after $\omega_{\rm pe}t \simeq 1000$, $W_\perp$ increases faster than $W_\parallel$ although $W_\perp$ oscillates with time. As a result, $W_\perp$ becomes greater than $W_\parallel$ after $\omega_{\rm pe}t \simeq 2000$. This indicates that the 2Ds positron gains energy from $E_\perp$ more than from $E_\parallel$.

As a result of the particle scattering by the 2D fluctuations, the energy gain from $E_\parallel$ is changed to that from $E_\perp$. The later stage of the acceleration is mainly due to the motional electric field in the wave frame, and the 2D fluctuation component of $E_\perp$ is much smaller than the motional electric field. As shown in Fig. 4, the 2D fluctuation amplitude $|\delta f_2|$ is smaller than $0.2B_0$. The δf_2 mainly consist of δE_{y2} and δB_{x2}, and the amplitude of δE_{y2} is smaller than that of δB_{x2} (for the details, see Ref. 14). This indicates that the 2D fluctuation component of $E_\perp$, which is almost equal to δE_{y2}, is at most $0.1B_0$, which is much smaller than the magnitude of the motional electric field, $v_{\rm sh}B_0/c \simeq 0.6B_0$, for this shock wave.

We now show orbits of other positrons. Most of the 1Dt positrons have orbits similar

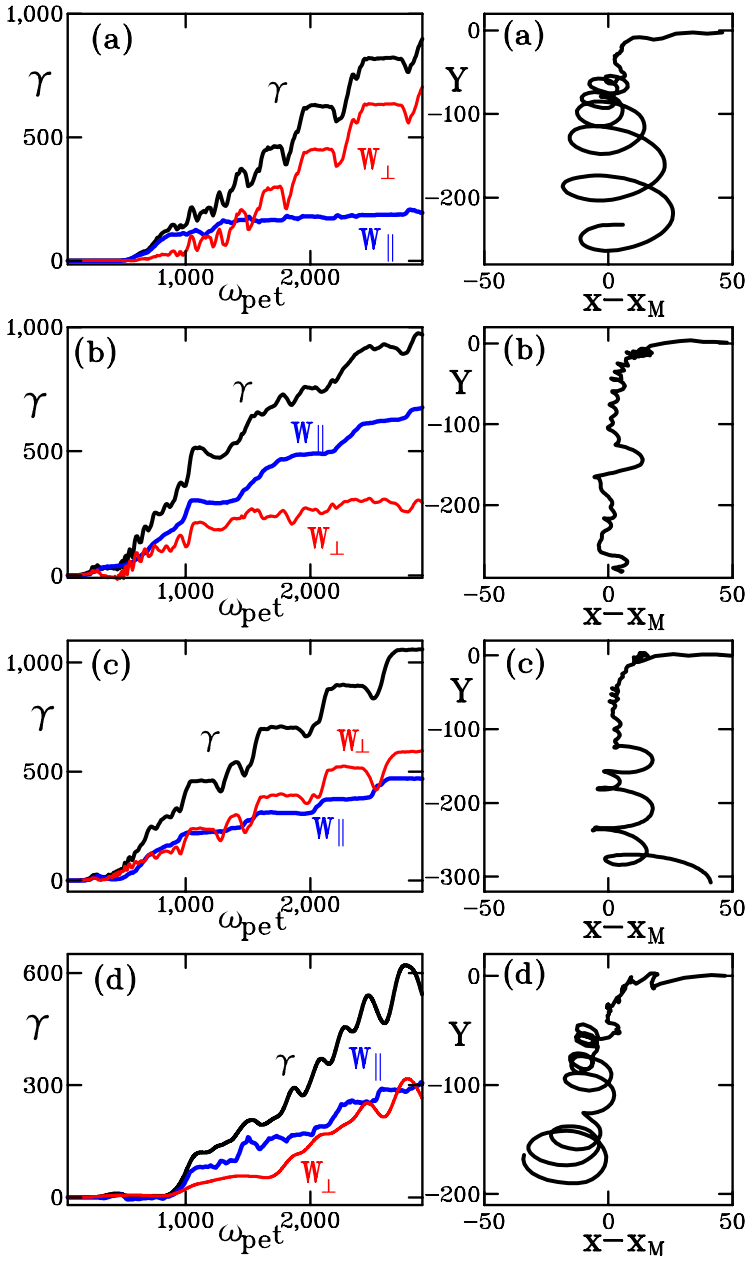

Fig. 8. Four types of orbits of 2Ds positrons (a)-(d). Time variations of γ, $W_{\parallel}$, and $W_{\perp}$ and orbits in the $(x - x_{\rm m}, y)$ plane are shown. The values of $x - x_{\rm m}$ and y are normalized by $c/\omega_{\rm pe}$, and the values of $W_{\parallel}$ and $W_{\perp}$ are normalized by $m_e c^2$. (Color online)

to the 1Dt positron orbit shown in Figs. 5-7. However, for the 2Ds positrons, we observed several types of orbits. Figure 8 displays the four types of orbits of the 2Ds positrons. The left panels show the time variations of γ, $W_{\parallel}$, and $W_{\perp}$, and the right panels show the orbits in

the $(x - x_m, y)$ plane where $x - x_m$ and y are normalized to $c/\omega_{\rm pe}$. The positron (a) is similar to the 2Ds positron shown in Figs. 5-7 and gains energy from $E_\perp$ more than from $E_\parallel$. Unlike the positron (a), the positron (b) continues to be accelerated by $E_\parallel$ until the end of the simulation and gains energy from $E_\parallel$ more than from $E_\perp$. The positron (b) stays near $x = x_m$ with a gyroradius much smaller than the positron (a) gyroradius. The positron (c) has the gyroradius that is between the gyroradii of the positron (a) and the positron (b). The values of $W_\parallel$ and $W_\perp$ of the positron (c) are approximately equal. The positron (c) orbit in the $(x - x_m, y)$ plane is similar to the curtate cycloid. The positron (d) is also accelerated by both $E_\parallel$ and $E_\perp$. However, the positron (d) goes deeply into the downstream region $x - x_{\rm M} < 0$ unlike the positrons (a), (b), and (c).

The orbits of the positrons (a), (b), and (c) shown in Fig. 8 are similar to the three types of orbits presented in Ref. 15, where the long time evolution of the positron acceleration was followed up to the time $\omega_{\rm pe}t = 5000$ by the 1D simulation and the effects of the nonstationarity of a shock wave were investigated. In the 1D simulation, the positrons were firstly accelerated by $E_\parallel$, and the three types of orbits appeared after the wave profile is considerably deformed due to the nonstationarity of the shock wave. However, in this 2D simulation, the 1D fluctuations due to the nonstationarity of the shock wave are small until the end of the simulation, as shown by Fig. 4, and the 2D fluctuations are much greater than the 1D fluctuations. Therefore, because of the 2D fluctuations, the three types of the 2Ds position orbits appeared. In addition, we find positrons that go deeply into the downstream region, such as the positron (d).

We also calcurate $W_\perp$ and $W_\parallel$ for many positrons. Figure 9 shows the positron distributions at $\omega_{\rm pe}t = 3000$ as functions of $W_\perp - W_\parallel$. Here, we consider the 1Dt positrons with $\gamma > 100$, the 2Ds positrons with $\gamma > 100$, and the 2Ds positrons with $\gamma > 500$. In the 1Dt positrons (the top panel), the number of the positrons with $W_\perp > W_\parallel$ is much smaller than the number of the positions with $W_\perp < W_\parallel$. This confirms that the 1Dt positrons are mainly accelerated by $E_\parallel$. In the 2Ds positrons with $\gamma > 100$ (the middle panel), the fraction of the positrons with $W_\perp > W_\parallel$ is increased compared to that in the 1Dt positrons with $\gamma > 100$. In the 2Ds positrons with $\gamma > 500$ (the bottom panel), the fraction of the positions with $W_\perp > W_\parallel$ is more than 60 %. This value is much greater than that for the 2Ds positrons with $\gamma > 100$. Thus, we confirm that the 2Ds positrons accelerated to higher energies tend to gain the energies from $E_\perp$ more than from $E_\parallel$ and the 2D fluctuations increase the number of such positrons.

Thus, as for the positron motions under the influence of the 2D fluctuations excited by the trapped electrons, we have shown the following characteristics. In addition to the accel-

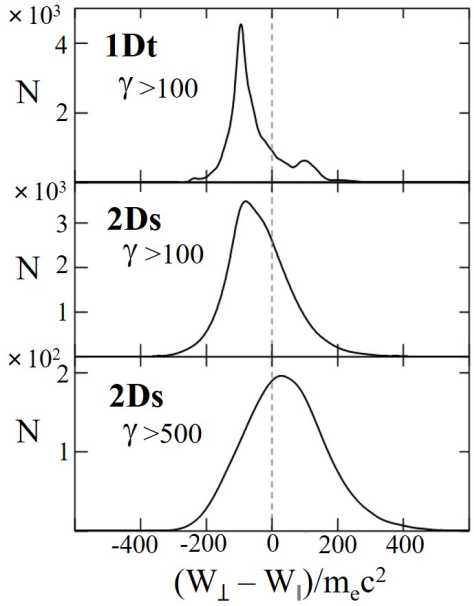

Fig. 9. Distributions of 1Dt positrons with $\gamma > 100$, 2Ds positrons with $\gamma > 100$, and 2Ds positrons with $\gamma > 500$ at $\omega_{pe}t = 3000$ as functions of $W_\perp - W_\parallel$.

eration by $E_\parallel$ in the shock transition region, some positrons can be accelerated by $E_\perp$ in the shock wave in association with the gyromotions. Although the 1D fluctuations due to the nonstationarity of the shock wave are small, several types of orbits depending on the positron gyroradius appear. The positrons accelerated to higher energies tend to gain energies from $E_\perp$ more than from $E_\parallel$.

3.4 Effects of positrons on 2D fluctuations

In this subsection, we consider effects of accelerated positrons on 2D fluctuations. Figure 10 shows the phase space plots of positrons and electrons and the contour maps of the 2D fluctuation of magnetic field B_x, δB_x, at $\omega_{pe}t = 680$ and 2610. At $\omega_{pe}t = 680$, the 2D fluctuation δB_x has large amplitude in the region near $x - v_{sh}t = 0$ where a large number of energetic electrons trapped in the shock wave exist. The number of energic positrons in this region is much smaller than that of the energetic electrons. Therefore, the 2D fluctuations are excited by the energetic electrons. However, at $\omega_{pe}t = 2610$, the 2D fluctuation δB_x have large amplitudes in the region $10 < (x - v_{sh}t)/(c/\omega_{pe}) < 30$ where there are more energetic positrons than energetic electrons.

As discussed in the previous paper,[14] the 2D fluctuations grow to large amplitudes as a result of nonlinear interaction between current filaments in the z direction. Figure 11 shows the contour maps of the electron current J_{ez} and the positron current J_{pz} at $\omega_{pe}t = 680$ and

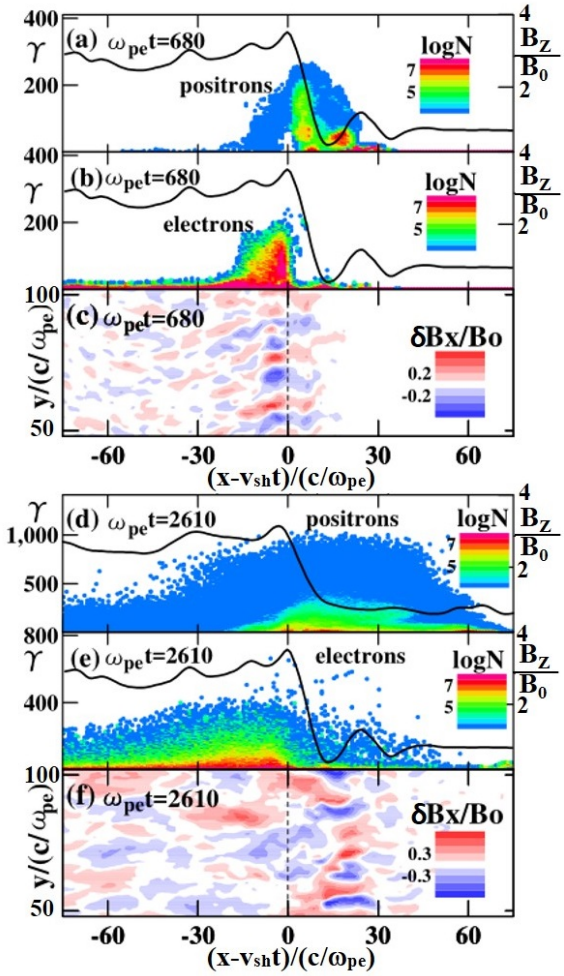

Fig. 10. Phase space plots of positrons and electrons and contour maps of the 2D fluctuation of B_x at $\omega_{pe}t$ = 680 and 2610. (Color online)

2610. Comparing Figs 10 (c), 11 (a) and (b), we see that at $\omega_{pe}t = 680$, the variation of δB_x along the y direction near $x - v_{sh}t = 0$ is related to that of $|J_{ez}|$. However, at $\omega_{pe}t = 2610$, as shown by Figs. 10 (f), 11 (c) and (d), the $|\delta B_x|$ is large in the region $10 < (x - v_{sh}t)/(c/\omega_{pe}) < 30$ where $|J_{ez}|$ is small and $|J_{pz}|$ is large, and the variation of δB_x along the y direction is related to that of $|J_{pz}|$. This indicates that at $\omega_{pe}t = 2610$, the 2D fluctuations are influenced by the accelerated positrons.

Figure 12(a) shows the time variation of the number of positrons with $\gamma > 100$ in the shock front region $0 < (x - v_{sh}t)/(c/\omega_{pe}) < 30$, where the positron number N_p is normalized by the number of electrons in the same region. The value of N_P increases with time. Figure 12(b) shows the time variation of x_{2D} that is the x position where the 2D fluctuation has the

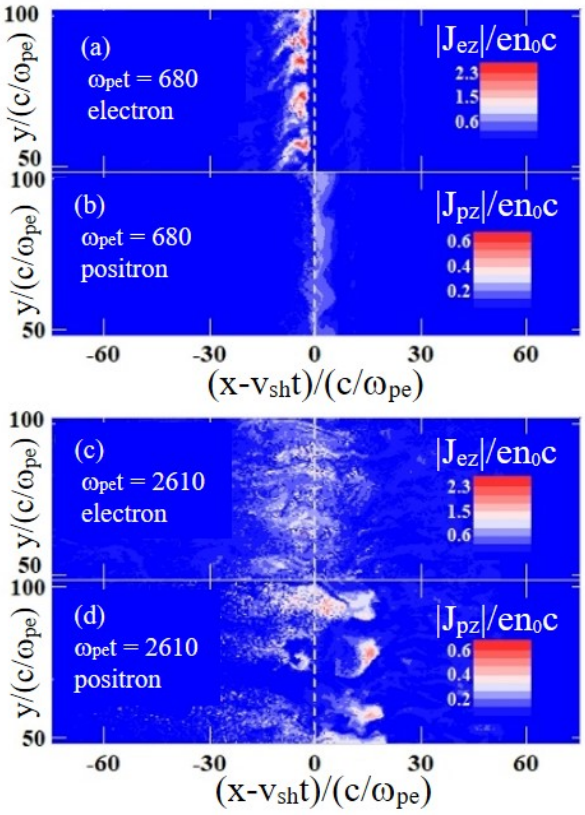

Fig. 11. Contour maps of the magnitudes of electron current J_{ez} and positron current J_{pz} at $\omega_{pe}t = 680$ and 2610. (Color online)

greatest amplitude. The values of $x_{2D} - v_{sh}t$ are normalized by c/ω_{pe}. For comparison, we plot the position x_{2D} obtained by the simulation for an electron-ion (e-i) plasma with the same parameters presented in Sec. II. The value of x_{2D} for the electron-ion-positron (e-i-p) plasma, shown by the black line, increases with time, whereas that for the e-i plasma (gray line) does not. We thus find that x_{2D} gradually shifts to the upstream region as the number of the accelerated positron increases.

As shown by Fig. 4, the 2D fluctuation amplitude $|\delta f_2|$ maintains large values after $\omega_{pe}t \simeq 2000$ although the number of trapped electrons gradually decreases. This is because the number of the accelerated positrons near the shock front increases with time and the positrons influence the 2D fluctuations. In the future, we will study effects of the 2D fluctuations influenced by the accelerated positrons on the motions of electrons, ions, and positrons by using long-time simulations.

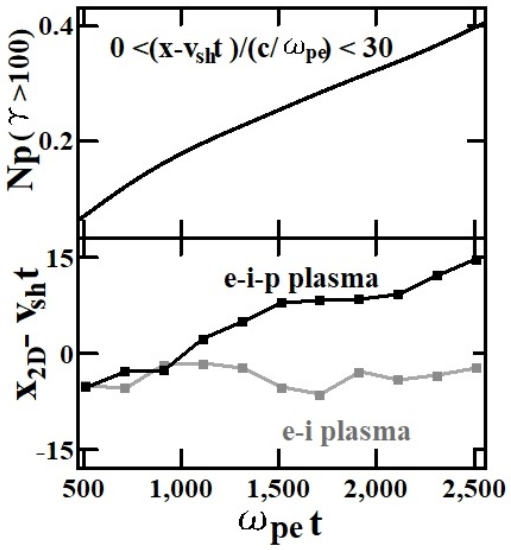

Fig. 12. Time variations of the number of energetic positrons with $\gamma > 100$ in the region $0 < (x - v_{\rm sh}t)/(c/\omega_{\rm pe}) < 30$ and of the x position at which the 2D fluctuation amplitude becomes the greatest. The value of N_p in the upper panel is normalized by the number of electrons in the same region. The gray line in the lower panel shows the result of the simulation for an electron-ion plasma.

4. Summary and Discussion

Some electrons can be trapped by a magnetosonic shock wave propagating obliquely to the external magnetic field and can excite electromagnetic fluctuations along the shock front, which we call 2D fluctuations. We studied effects of the 2D fluctuations on positron acceleration by a shock wave in an electron-ion-positron plasma with a small positron density.

First, we performed a shock wave simulation using a two-dimensional electromagnetic particle code. The shock wave propagates in the x direction in the external magnetic field, $\boldsymbol{B}_0 = (B_0 \cos\theta, 0, B_0 \sin\theta)$, with the speed $v_{\rm sh} \simeq c\cos\theta$. We followed the orbits of a large number of positrons, which we call 2Ds positrons. We also calculated the motions of the same number of test positrons in the y-averaged electromagnetic fields obtained by the 2D simulation. That is, the test positrons, which we call 1Dt positions, are not influenced by the 2D fluctuations.

We showed that both the 1Dt positrons and the 2Ds positrons are accelerated to ultrarelativistic energies. This indicates that the ultrarelativistic positron acceleration can occur even when the 2D fluctuations excited by the trapped electrons grow to large amplitudes. Further, the comparison between the 2Ds positrons and the 1Dt positrons elucidated the effects of the 2D fluctuations on the positron acceleration. The 2Ds positrons are accelerated to higher energies than the 1Dt positrons. The accelerated 2Ds positrons are distributed over a wide

region from the upstream to the downstream of the shock wave, whereas almost all of the accelerated 1Dt positrons are in the upstream region near the shock front.

As for the acceleration mechanism, it was shown that in addition to the parallel electric field $E_{\parallel}$ in the shock transition region, the perpendicular electric field $E_{\perp}$ in the shock wave greatly contributes to the acceleration of the 2Ds positrons. When the 1Dt positrons and the 2Ds positrons encounter the shock wave, they are accelerated by $E_{\parallel}$ in the shock transition region. Then, almost all of the 1Dt positrons are reflected to the upstream region and their energies do not increase any further. On the other hand, even after the acceleration by $E_{\parallel}$, some of the 2Ds positrons continue to gain energies from $E_{\perp}$ in the shock wave because they can enter and exit the shock wave in association with the gyromotions. We also showed that several types of the 2Ds positron orbits depending on the gyroradius appear although the nonstationarity of the shock wave is small. By analyzing the works done by $E_{\parallel}$ and $E_{\perp}$ for many positrons, it was found that the 2Ds positrons accelerated to higher energies tend to gain energies from $E_{\perp}$ more than from $E_{\parallel}$.

We also discussed effects of the accelerated positrons on 2D fluctuations. It was shown that the position where the 2D fluctuation amplitude becomes large gradually shifts to the upstream region as the number of the accelerated positrons increases.

We note that fluctuations and waves in the shock transition region play important roles in the other acceleration mechanism. In Refs. 29–31 , the authors studied effects of the fluctuations on the conventional shock drift acceleration (SDA), in which a particle gains energy from the motional electric field while drifting along the shock surface in the shock transition region. They showed that the presence of the fluctuations can significantly enhance the efficiency of the SDA because the particles can be confined in the shock transition region for a long time as a result of the scattering by the fluctuations. This acceleration is called the stochastic shock drift acceleration (SSDA). They considered shock waves in relatively high beta plasmas such that $\beta \geq 1$ in the upstream region, whereas we considered a shock wave in a low beta plasma $\beta \sim 10^{-3}$. Also, the role of the fluctuations shown in this paper is different from that for the SSDA. (In this acceleration, the energy gain from $E_{\parallel}$ is changed to that from $E_{\perp}$ as a result of the scattering by the fluctuations, and the confinement of particles near the shock front is caused by the shock condition $v_{\rm sh} \simeq c\cos\theta$.) Thus, there are many differences between the SSDA and this acceleration. However, it is very interesting that the fluctuations in the shock transition region hold the key to the efficiency for both of the two acceleration mechanisms. If we can clarify how this acceleration changes as the plasma beta increases, we may obtain a clue to understand the relation between this acceleration and the SSDA.

Acknowledgment

This work is performed on "Plasma Simulator" (FUJITSU FX100) of NIFS with the support and under the auspices of the NIFS Collaboration Research program (NIFS18KNXN367). Development of some numerical codes used in this work was supported in part by the "Code development support program" of Numerical Simulation Reactor Research Project (NSRP), NIFS. This work was supported in part by a Grant-in-Aid for Scientific Research (C) Grant No.15K05367 of Japan Society for the Promotion of Science and by "Joint Usage/Research Center for Interdisciplinary Large-scale Information Infrastructures" in Japan (Project ID: jh1900007-NAH)..

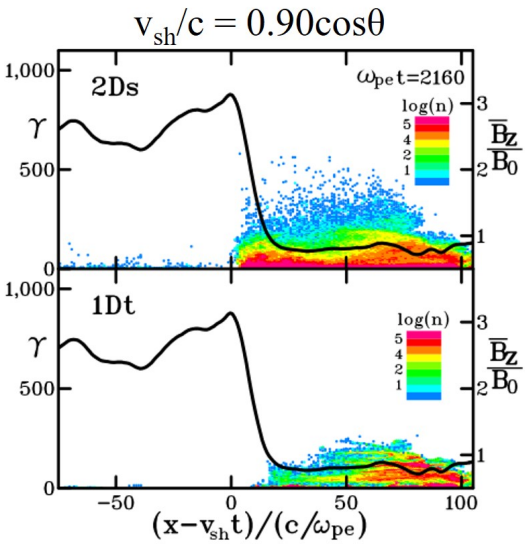

Fig. 13. Phase spaces (x, γ) of the 2Ds positrons and the 1Dt positrons and the x profile of the y-averaged magnetic field $\bar{B}_z$ of the shock wave with $v_{\rm sh} = 0.90c\cos\theta$ at $\omega_{\rm pe}t = 2160$. (Color online)

Appendix

In Sec. III, we analyzed the positron motions in the shock wave with $v_{\rm sh} = 0.95c\cos\theta$. In this appendix, we present the positron distributions in the shock waves with a little smaller $v_{\rm sh}$ and a little greater $v_{\rm sh}$, $v_{\rm sh} = 0.90c\cos\theta$ and $1.05c\cos\theta$.

Figure 13 shows the phase space (x, γ) of 2Ds positrons and 1Dt positrons in the shock wave with $v_{\rm sh} = 0.90c\cos\theta$ at $\omega_{\rm pe}t = 2160$. The 2Ds positrons are accelerated to higher energies than the 1Dt positrons, although the positron acceleration is weaker when $v_{\rm sh} =$

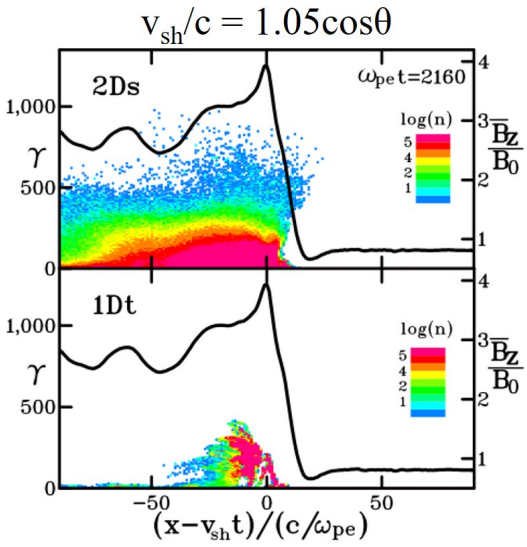

Fig. 14. Phase spaces (x, γ) of the 2Ds positrons and the 1Dt positrons and the x profile of the y-averaged magnetic field $\bar{B}_z$ of the shock wave with $v_{\rm sh} = 1.05c\cos\theta$ at $\omega_{\rm pe}t = 2160$ (Color online)

$0.90c\cos\theta$ than when $v_{\rm sh} = 0.95c\cos\theta$ (see Fig. 2). Unlike in Fig. 2, there are few energetic positrons in the region $x < v_{\rm sh}t$ in Fig. 13. This is because the positrons accelerated to $v_{\parallel} \simeq c$ can easily go ahead of the shock wave because their velocities in the x direction, $v_x \simeq c\cos\theta$, are sufficiently greater than the shock speed, $v_{\rm sh} = 0.90c\cos\theta$.

Figure 14 shows the positron phase space (x, γ) at $\omega_{\rm pe}t = 2160$ for the shock wave with $v_{\rm sh} = 1.05c\cos\theta$. Unlike when $v_{\rm sh}$ is a little smaller than $c\cos\theta$, almost all the accelerated 1Dt positrons are in the region $x < v_{\rm sh}t$ when $v_{\rm sh} = 1.05c\cos\theta$. This is because the positrons accelerated to $v_{\parallel} \simeq c$ can be easily overtaken by the shock wave. Compared to the 1Dt positrons, the 2Ds positrons are accelerated to higher energies and the energetic 2Ds positrons are distributed over the wider region although there are few energetic 2Ds positrons in the region $x > v_{\rm sh}t$.

References

1) R. Z. Sagdeev: in Reviews of Plasma Physics, ed. M. A. Leontovich (Consultants Bureau, New York, 1966) Vol. 4, p. 23.

2) D. A. Tidman and N. A. Krall: Schock Waves in Collisionless Plasmas (Wiley, New York, 1971).

3) Y. Ohsawa, Phys. Reports **536**, 147 (2014).

4) N. Bessho and Y. Ohsawa, Phys. Plasmas **6**, 3076 (1999).

5) N. Bessho and Y. Ohsawa, Phys. Plasmas **9**, 979 (2002).

6) H. Hasegawa, S. Usami, and Y, Ohsawa, Phys. Plasmas **10**, 3455 (2003).

7) H. Hasegawa and Y. Ohsawa, Phys. Plasmas **12**, 012312 (2005).

8) P. A. Sturrock, Astrophys. J. **164**, 529 (1971).

9) C. F. Kennel and R. Pellat, J. Plasma Phys. 15, 335 (1976).

10) A. M. Atoyan, F. A. Aharonian, and H. J. V ölk, Phys. Rev. D, **52**, 3265 (1995).

11) N. Kawanaka, K. Iota, and N. M. Nojiri, Astrophys. J. **710** 958 (2010).

12) A. Zindo, Y. Ohsawa, N. Bessho, and R. Sydora, Phys. Plasmas **12** 052321 (2005).

13) K. Shikii and M. Toida, Phys. Plasmas **17**, 082316 (2010).

14) M. Toida and J. Joho, J. Phys. Soc. Jpn. **81**, 084502 (2012).

15) H. Hasegawa, K. Kato and Y. Ohsawa, Phys. Plasmas **12**, 082306 (2005)

16) T. Iwata, S. Takahashi, and Y. Ohsawa, Phys. Plasmas **19**, 022302 (2012).

17) P. C. Liewer, A. T. Lin, J. M. Dawson, and M. Z. Caponi, Phys. Fluids **24**, 1364 (1981).

18) S. Takahashi and Y. Ohsawa, Phys. Plasmas **14**, 112305 (2007); S. Takahashi, M. Sato, and Y. Ohsawa, Phys. Plasmas **15**, 082309 (2008).

19) M. Toida, Phys. Plasmas **23**, 072115 (2016).

20) S. Usami and Y. Ohsawa, Phys. Plasmas **9**, 1069 (2002).

21) J. H. Adlam and J. E. Allen, Philos. Mag., Suppl. **3**, 448 (1958).

22) L. Davis, R. Lüst, and A. Schlüter, Z. Naturforsch. A **13**, 916 (1958).

23) C. S. Gardner and G. K. Morikawa, Commun. Pure Appl. Math. **18**, 35 (1965).

24) T. Kakutani, H. Ono, T. Taniuti, and C. C. Wei, J. Phys. Soc. Jpn. **24**, 1159 (1968).

25) T. Kawashima, S. Miyahara, and Y. Ohsawa, J. Phys. Soc. Jpn. **72**, 1164 (2003).

26) C. S. Morawetz, Phys. Fluids **4**, 988 (1961).

27) D. Biskamp and H. Welter, Nucl. Fusion **12**, 663 (1972).

28) M. Toida and J. Inagaki, Phys. Plasmas, **22**, 062305 (2015).

29) Y. Matsumoto, T., Amano, T. N. Kato, and M. Hoshino, Phys. Rev. Lett. **119**, 105101 (2017).

30) O. Kobzar, J. Niemiec, T. Amano, M. Hoshino, S. Matsukiyo, Y. Matsumoto, and M. Pohl, in Proceedings of Science **358**, 368 (2019).

31) T. Katou and T. Amano, Astrophys. J. **874**, 119 (2019).